frontiers | Frontiers in Physics

ORIGINAL RESEARCH
published: 25 May 2022
doi: 10.3389/fphy.2022.927907

Calculation of the Coupling Coefficient in Step-Index Multimode Polymer Optical Fibers Based on the Far-Field Measurements

***Svetislav Savović*[1,2]*, Alexandar Djordjevich*[3]*, Branko Drljača*[4]*, Ana Simović*[2] *and Rui Min*[1]*

[1]Center for Cognition and Neuroergonomics, State Key Laboratory of Cognitive Neuroscience and Learning, Beijing Normal University, Zhuhai, China, [2]Faculty of Science, University of Kragujevac, Kragujevac, Serbia, [3]Department of Mechanical Engineering, City University of Hong Kong, Kowloon, China, [4]Faculty of Sciences, University of Priština in Kosovska Mitrovica, Kosovska Mitrovica, Serbia

Using the power flow equation (PFE), this article investigates mode coupling in step-index (SI) multimode (MM) polymer optical fiber (POF). This equation's coupling coefficient was initially fine-tuned so that it could appropriately reconstruct previously recorded far-field (FF) power distributions. The equilibrium mode distribution (EMD) and steady-state distribution (SSD) in the SI MM POF were found to be obtained at lengths $L_c = 15$ m and $z_s = 41$ m, respectively. These lengths are substantially shorter than their glass optical fiber counterparts. Such characterization of the investigated POF can be used in its employment as a part of the communication or sensory system. Namely, the POF's bandwidth is inverse linear function of fiber length (z^{-1}) below the coupling length L_c. However, it has a $z^{-1/2}$ dependence beyond this equilibrium length. Thus, the shorter the coupling length L_c, the sooner transition to the regime of slower bandwidth decrease occurs. It is also important to be able to determine a modal distribution at a certain length of the POF employed as a part of optical fiber sensory system.

Keywords: polymer optical fiber, modal distribution, coupling length, bandwidth, distance dependence, sensory system

OPEN ACCESS

Edited by:
Sushank Chaudhary, Quanzhou Institute of Equipment Manufacturing (CAS), China

Reviewed by:
Lei Liu, Harbin Engineering University, China
Yuyang Peng, Macau University of Science and Technology, Macao SAR, China

****Correspondence:***
Rui Min
ruimin@bnu.edu.cn

Specialty section:
This article was submitted to Optics and Photonics, a section of the journal Frontiers in Physics

Received: *25 April 2022*
Accepted: *09 May 2022*
Published: *25 May 2022*

Citation:
Savović S, Djordjevich A, Drljača B, Simović A and Min R (2022) Calculation of the Coupling Coefficient in Step-Index Multimode Polymer Optical Fibers Based on the Far-Field Measurements. Front. Phys. 10:927907. doi: 10.3389/fphy.2022.927907

INTRODUCTION

Silica optical fiber has a lot of advantages such as a low loss, lightweight, and high bandwidth [1–4]. Although silica optical fiber has a lot of advantages, is not appropriate for short-distance applications such as automotive [5], local area networks [6], and visible light communication (VLC) applications [7]. On the other hand, POFs are made of poly (methylmethacrylate) (PMMA) [8, 9], polycarbonate (PC) [10, 11], ZEONEX ® [12, 13], TOPAS ® [14, 15], poly dimethyl siloxane (PDMS) [16, 17] or hydrogel [18, 19].

Apart from optical fiber material, optical fibers usually have step-index or graded-index refractive index distribution, and can operate in a single-mode or multimode regime. There are several typical commercial POFs, such as Mitsubishi Rayon's Eska Extra EH 4001 SI MM POF [20] and CYTOP® graded index (GI) POF [21], both of them could transmit a large number of modes, and have been used for short-range communications and sensing area in fiber optic sensory systems [22]. Additionally, micro-structured polymer optical fiber which was first produced by Argyros' group, is one very specific type of POF [23]. However, due to the transmission loss and butt-coupling with commercial silica optical fiber, only one Start-up Company supplied the commercial

FIGURE 1 | Schematics of measuring FF power distributions.

product [24]. PMMA SI MM POF is still the most common one with lots of commercial products on the market.

Mode coupling has a significant impact on the transmission performance of PMMA SI MM POF. The transfer of power between nearby modes is represented by such coupling. It causes the launched light's angular power distribution to be disrupted [25, 26]. It is caused by the optical fiber's intrinsic perturbation effects (for example, variations of the refractive index distribution and microscopic bends). The angular power distribution is predicted to be influenced by the launch conditions and mode coupling characteristics. Thus, a Gaussian beam launched at an angle θ_0 in respect to the optical fiber axis, at the output end of a short piece of optical fiber, is seen as a sharp ring pattern (the ring diameter depends on θ_0). Mode coupling, on the other hand, causes such a ring pattern to be distorted in longer fibers and finally transformed into disk. The coupling length L_c marks the fiber length at which the ring pattern of the highest order guiding mode evolved into disk, indicating that an EMD is established. Coupling can fully complete at optical fiber length z_s ($z_s > L_c$), which is referred to as an SSD.

The light transmission performance of PMMA SI MM POF is investigated in this work. The modal power diffusion model is used to obtain the coupling coefficient D. In this way, we computed the L_c required to accomplish the EMD and the length z_s to achieve the SSD. By such a characterization of mode coupling process in an optical fiber one can predict at which length $z = L_c$ one can expect that bandwidth decrease with length would start to decelerate, as explained in more details in Results and Discussion. It is also important to know the state of mode coupling in an optical fiber employed as a part of optical fiber sensory system, especially in terms of the modal distribution at certain fiber length.

POWER FLOW EQUATION

The Gloge's PFE has the following form [27]:

$$\frac{\partial P(\theta,z)}{\partial z} = -\alpha(\theta)P(\theta,z) + \frac{D}{\theta}\frac{\partial}{\partial\theta}\left(\theta\frac{\partial P(\theta,z)}{\partial\theta}\right) \quad (1)$$

where $P(\theta, z)$ is the angular power distribution, θ is the angle of propagation, z is the distance of the propagation, D is the coupling coefficient (assumed constant [27, 28]) and $\alpha(\theta)$ is the modal attenuation. **Eq. 1** can be reduced to [29]:

$$\frac{\partial P(\theta,z)}{\partial z} = \frac{D}{\theta}\frac{\partial P(\theta,z)}{\partial\theta} + D\frac{\partial^2 P(\theta,z)}{\partial\theta^2} \quad (2)$$

Steady-state solution of **Eq. 2** is given as [28]:

$$P(\theta,z) = J_0\left(2.405\frac{\theta}{\theta_c}\right)\exp(-\gamma_0 z) \quad (3)$$

where J_0 is the Bessel function of the first and zero-order, γ_0 [m^{-1}] = $2.405^2 D/\theta c^2$ is the attenuation coefficient. In this work, solved **Eq. 2** using the explicit finite difference method [29].

In our earlier published work, we proposed a method which enables that the coupling coefficient D can be obtained from just two output angular power distributions $P(\theta, z)$ in the case of centrally launched beam [30]. As an alternative, in this work we propose a method for calculating the coupling coefficient D on the basis of the measured FFPs $p(x, z)$, illustrated in **Figure 1**.

RESULTS AND DISCUSSION

We used the PFE (2) to calculate the lengths L_c and z_s for the POF that Ribeiro et al. [31] studied experimentally. This POF (Mitsubishi Rayon's Eska Extra EH 4001) had NA = 0.47, the inner critical angle $\boldsymbol{\theta_c}$ = 18° ($\boldsymbol{\theta_c}$ = 27.4° measured in air), core

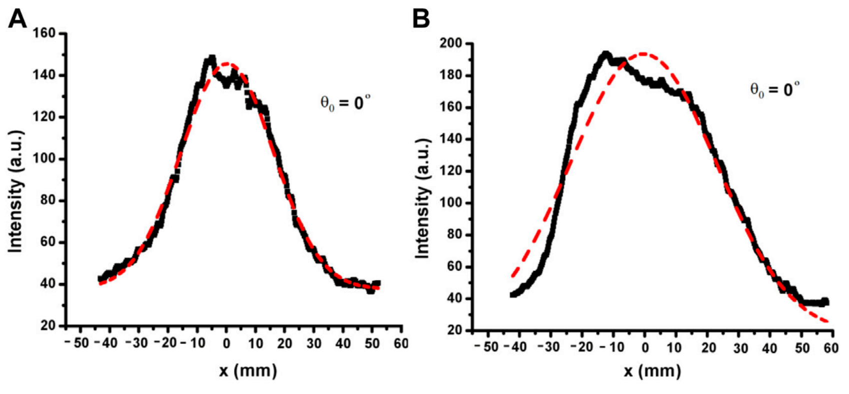

FIGURE 2 | The measured FF pattern from **(A)** ~1 m and **(B)** ~19 m PMMA SI MM POF lengths. The light was launched at θ_0 = 0° [31].

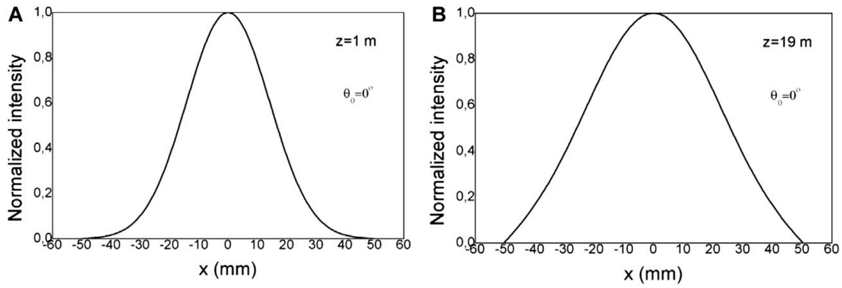

FIGURE 3 | Normalized output power distribution P (x, z = 1 and 19 m, L = 110 mm) at the end of **(A)** 1 m and **(B)** 19 m long PMMA SI MM POF, obtained by solving the PFE for Gaussian launch distribution with input angle $\theta_0 = 0°$, obtained from the P (x, z = 1 and 19 m, L = 110 mm), for $x = L{\cdot}tg\theta$, where L is the receiving distance.

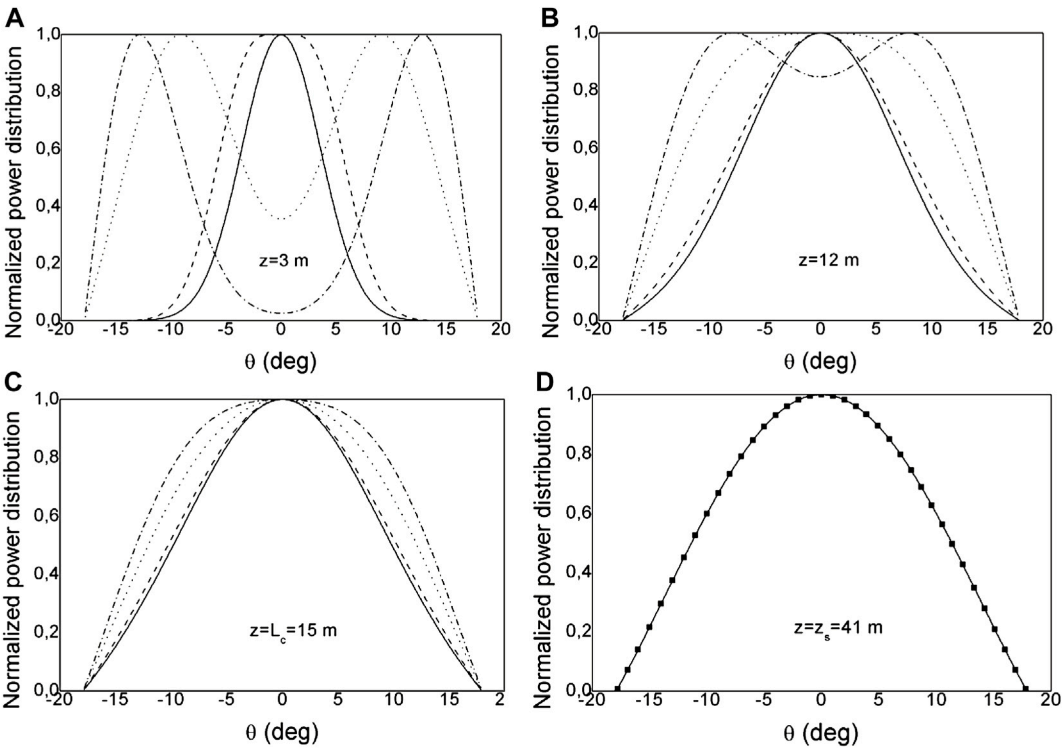

FIGURE 4 | The normalized angular power distribution at the end of PMMA SI MM POF, obtained by solving the PFE for four Gaussian launch distributions with input angles $\theta_0 = 0^o$ (—), $\theta_0 = 5^o$ (– –), $\theta_0 = 10^o$ (●●●) and $\theta_0 = 15^o$ (–●–), with $(FWHM)_{z=0} = 7^o$ (g represent the analytical SSD).

refractive index $n_{core} = 1.4897$, numerical aperture NA = 0.46 and fiber diameter d = 1 mm. Ribeiro et al. focused a He-Ne laser beam at 633 nm onto the input end of the fiber in their experiment (**Figure 1**). They used a CCD to detect the FF patterns of the fiber output.

The coupling coefficient D is obtained by its fine-tuning in the PFE, thus recreating the Ribeiro et al.'s measured FF patterns in this fiber for lengths of z = 1 m and z = 19 m (**Figure 2**). This necessitated numerically calculating the PFE for various values of D. The value of $D = 9.2 \times 10^{-4}$ rad^2/m enabled the best fit between the calculated and measured output power distributions.

A Gaussian launch beam with $(FWHM)_{z=0} = 7^o$ is used in the computations. **Figure 3** shows the output power distribution for a z = 1 and 19 m length POF with an input angle of $\theta_0 = 0^o$ obtained as numerical solution of **Eq. 2**. The distributions P (x, z = 1 and 19 m, L = 110 mm) are generated from the distributions P (θ, z = 1 and 19 m, L = 110 mm), where $x = L{\cdot}tg\theta$ and L is the receiving distance.

In **Figure 4**, our numerical results for the normalized output angular power distribution for input angles θ_0 = 0, 5, 10, and 15^o are shown. At short fiber lengths, a significant mode coupling is observed for low order modes, as can be seen in **Figure 4A**. The EMD is achieved at length $z = L_c$ = 15 m (**Figure 4C**), while the SSD is established at z_s = 41 m in **Figure 4D**.

The coupling coefficient D for the PMMA SI MM POF evaluated in this work is similar to those which we obtained for other investigated POFs (~10^{-4} rad^2/m), so the characteristic lengths for coupling, L_c and z_s, are similar (L_c is between ≃15–35 m and z_s is between ≃40 and 100 m [25, 29, 30]). We have previously reported that glass optical fibers show the weakest strength of mode coupling ($D \sim 10^{-7}$ to 10^{-6} rad^2/m), so their SSD lengths z_s are between ≃ 1–10 km [32].

It is worth noting that the length dependence of the bandwidth of POF is determined by mode coupling behavior. The bandwidth is inverse linear function of fiber length (z^{-1}) below the coupling length L_c. However, it has a $z^{-1/2}$ dependence beyond this equilibrium length. Thus, the shorter the coupling length L_c, the sooner transition to the regime of slower bandwidth decrease occurs [26]. It is obvious that mode coupling has a beneficial influence on bandwidth. Therefore, it is of great interest to characterize mode coupling in an optical fiber in order to predict its transmission characteristics, especially to determine at which coupling length L_c one can expect that bandwidth would start to improve. It is also important to know the state of mode coupling in an optical fiber employed as a part of optical fiber sensory system, especially in terms of the modal distribution at certain fiber length.

CONCLUSION

We investigate a mode coupling along a PMMA SI MM POF previously investigated experimentally by Ribeiro et al. [31]. To appropriately recreate the measured FF patterns reported before, the coupling coefficient D in the PFE is tweaked. As a result, the lengths L_c and z_s that characterize the coupling process are obtained. Such characterization of the investigated PMMA SI MM POF can be used in its employment as a part of communication or sensory system. In practice, by characterization of mode coupling in an optical fiber one can predict its transmission characteristics, especially to determine length-dependent bandwidth behavior. Since POF's bandwidth is inverse linear function of fiber length (z^{-1}) below the coupling length L_c, while it has a $z^{-1/2}$ dependence beyond this equilibrium length, it is obvious that the shorter the coupling length L_c leads to the sooner transition to the regime of slower bandwidth decrease. It is also important to be able to determine a modal distribution at a certain length of the fiber employed as a part of optical fiber sensory system.

DATA AVAILABILITY STATEMENT

The original contributions presented in the study are included in the article/supplementary material, further inquiries can be directed to the corresponding author.

AUTHOR CONTRIBUTIONS

SS: methodology, conceptualization, formal analysis, validation, writing—original draft. RM: conceptualization, formal analysis, funding acquisition, writing—review and editing. AD: formal analysis, validation, writing—review and editing. BD: validation, writing—review and editing. AS: validation, writing—review and editing.

FUNDING

This research was funded by the National Natural Science Foundation of China (62003046, 6211101138); the Strategic Research Grant of City University of Hong Kong (Project No. CityU 7004600); Serbian Ministry of Education, Science and Technological Development (Agreement No. 451-03-68/2020-14/200122); Science Fund of the Republic Serbia (Agreement No. CTPCF-6379382); Guangdong Basic and Applied Basic Research Foundation (2021A1515011997); The Innovation Team Project of Guangdong Provincial Department of Education (2021KCXTD014); Special project in the key field of Guangdong Provincial Department of Education (2021ZDZX1050).

REFERENCES

1. Min R, Liu Z, Pereira L, Yang C, Sui Q, Marques C. Optical Fiber Sensing for marine Environment and marine Structural Health Monitoring: A Review. *Opt Laser Techn* (2021) 140:107082. doi:10.1016/j.optlastec.2021.107082
2. Xiang M, Fu S, Xu O, Li J, Peng D, Gao Z, et al. Advanced DSP Enabled C-Band 112 Gbit/s/λ PAM-4 Transmissions with Severe Bandwidth-Constraint. *J Lightwave Technol* (2022) 40(4):987–96. doi:10.1109/jlt.2021.3125336
3. Maeda H, Saito K, Sasai T, Hamaoka F, Kawahara H, Seki T, et al. Real-time 400 Gbps/carrier WDM Transmission over 2,000 Km of Field-Installed G654E Fiber. *Opt Express* (2020) 28(2):1640–6. doi:10.1364/oe.383471
4. Li Y, Fan H, Zhang L, Wang K, Wu G, Liu Z. A bend-tolerant BOTDR Distributed Fiber Sensor. *Opt Commun* (2022) 514:128110. doi:10.1016/j.optcom.2022.128110
5. POF automotive application. Automotive (2022). Available at: https://www.kdpof.com/automotive/(Access on 04 02, 2022).
6. Forni F, Shi Y, Tran N-C, Van Den Boom H, Tangdiongga E, Koonen T. Multi-Format Wired and Wireless Signals over Large-Core Plastic Fibers for in-home Network. *J Lightwave Technol* (2018) 36:1. doi:10.1109/JLT.2018.2839029
7. Apolo JA, Ortega B, Almenar V, Almenar V. Hybrid POF/VLC Links Based on a Single LED for Indoor Communications. *Photonics* (2021) 8(7):254. doi:10.3390/photonics8070254
8. Liu L, Zheng J, Deng S, Yuan L, Teng C. Parallel Polished Plastic Optical Fiber-Based SPR Sensor for Simultaneous Measurement of RI and Temperature. *IEEE Trans Instrum Meas* (2021) 70:1–8. doi:10.1109/TIM.2021.3072136
9. Hu X, Woyessa G, Kinet D, Janting J, Nielsen K, Bang O, et al. BDK-doped Core Microstructured PMMA Optical Fiber for Effective Bragg Grating Photo-Inscription. *Opt Lett* (2017) 42(11):2209–12. doi:10.1364/ol.42.002209
10. Zubel MG, Fasano A, Woyessa GT, Min R, Leal-Junior AG, Theodosiou A, et al. Bragg Gratings Inscribed in Solid-Core Microstructured Single-Mode Polymer Optical Fiber Drawn from a 3D-Printed Polycarbonate Preform. *IEEE Sensors J* (2020) 20(21):12744–57. doi:10.1109/JSEN.2020.3003469
11. Moslan MS, Othman MHD, Samavati A, Salim MAM, Rahman MA, Ismail AF, et al. Fabrication of Polycarbonate Polymer Optical Fibre Core via Extrusion Method: The Role of Temperature Gradient and Collector Speed

on its Characteristics. *Opt Fiber Techn* (2020) 55:102162. doi:10.1016/j.yofte.2020.102162
12. Woyessa G, Rasmussen HK, Bang O. Zeonex - a Route towards Low Loss Humidity Insensitive Single-Mode Step-index Polymer Optical Fibre. *Opt Fiber Techn* (2020) 57:102231. doi:10.1016/j.yofte.2020.102231
13. Dash JN, Cheng X, Gunawardena DS, Tam H-Y. Rectangular Single-Mode Polymer Optical Fiber for Femtosecond Laser Inscription of FBGs. *Photon Res* (2021) 9(10):1931–8. doi:10.1364/prj.434252
14. Marques CAF, Min R, Junior AL, Antunes P, Fasano A, Woyessa G, et al. Fast and Stable Gratings Inscription in POFs Made of Different Materials with Pulsed 248 Nm KrF Laser. *Opt Express* (2018) 26(2):2013–22. doi:10.1364/oe.26.002013
15. Markos C, Stefani A, Nielsen K, Rasmussen HK, Yuan W, Bang O. High-T_g TOPAS Microstructured Polymer Optical Fiber for Fiber Bragg Grating Strain Sensing at 110 Degrees. *Opt Express* (2013) 21(4):4758–65. doi:10.1364/oe.21.004758
16. Leal-Junior A, Guo J, Min R, Fernandes AJ, Frizera A, Marques C. Photonic Smart Bandage for Wound Healing Assessment. *Photon Res* (2021) 9(3):272–80. doi:10.1364/prj.410168
17. Shentu Z, Kang J, Zhu Z, Wang L, Guo Y, Xu T, et al. No-core PDMS Fiber for Large-Scale Strain and Concentration Measurement. *Opt Fiber Techn* (2021) 63:102531. doi:10.1016/j.yofte.2021.102531
18. Elsherif M, Hassan MU, Yetisen AK, Butt H. Hydrogel Optical Fibers for Continuous Glucose Monitoring. *Biosens Bioelectron* (2019) 137(15):25–32. doi:10.1016/j.bios.2019.05.002
19. Guo J, Liu X, Jiang N, Yetisen AK, Yuk H, Yang C, et al. Highly Stretchable, Strain Sensing Hydrogel Optical Fibers. *Adv Mater* (2016) 28(46):10244–9. doi:10.1002/adma.201603160
20. Mitsubishi POF SH4001. Ibsstore (2022). Available at: https://www.ibselectronics.com/ibsstore/sh4001-mitsubishi-rayon-eska-plastic-optical-fiber-cable.html (Access on 04 02, 2022).
21. Woyessa G, Theodosiou A, Markos C, Kalli K, Bang O. Single Peak Fiber Bragg Grating Sensors in Tapered Multimode Polymer Optical Fibers. *J Lightwave Technol* (2021) 39(21):6934–41. doi:10.1109/JLT.2021.3103284
22. He R, Teng C, Kumar S, Marques C, Min R. Polymer Optical Fiber Liquid Level Sensor: A Review. *IEEE Sensors J* (2022) 22(2):1081–91. doi:10.1109/jsen.2021.3132098
23. van Eijkelenborg M, Large M, Argyros A, Zagari J, Manos S, Issa N, et al. Microstructured Polymer Optical Fibre. *Opt Express* (2001) 9(7):319–27. doi:10.1364/oe.9.000319
24. Shute Company. Shute (2022). Available at: https://shute.dk/(Access on 04 02, 2022).
25. Savović S, Djordjevich A. Mode Coupling in Strained and Unstrained Step-index Plastic Optical Fibers. *Appl Opt* (2006) 45:6775–80. doi:10.1364/AO.45.006775
26. Mateo J, Losada MA, Zubia J. Frequency Response in Step index Plastic Optical Fibers Obtained from the Generalized Power Flow Equation. *Opt Express* (2009) 17:2850–60. doi:10.1364/oe.17.002850
27. Gambling WA, Payne DN, Matsumura H. Mode Conversion Coefficients in Optical Fibers. *Appl Opt* (1975) 14:1538–42. doi:10.1364/ao.14.001538
28. Rousseau M, Jeunhomme L. Numerical Solution of the Coupled-Power Equation in Step-Index Optical Fibers. *IEEE Trans Microwave Theor Techn.* (1977) 25:577–85. doi:10.1109/TMTT.1977.1129162
29. Djordjevich A, Savovic S. Investigation of Mode Coupling in Step index Plastic Optical Fibers Using the Power Flow Equation. *IEEE Photon Technol Lett* (2000) 12:1489–91. doi:10.1109/68.887704
30. Savović S, Djordjevich A. Method for Calculating the Coupling Coefficient in Step-index Optical Fibers. *Appl Opt* (2007) 46:1477–81. doi:10.1364/AO.46.001477
31. Ribeiro R, Silva V, Balod Y, Barbero AP, Germano S, Santos Pd. *Profile Scanning Measurements of Far-Field from Plastic Optical Fibre (POF) Passive Devices for Bandwidth Characterization in Datacom Networks*. Rio de Janeiro: XXVI Simposio Brasileiro de Telecomunicaciones-BrT´ (2008). p. 08. doi:10.14209/sbrt.2008.42632
32. Djordjevich A, Savović S, Tse PW, Drljača B, Simović A. Mode Coupling in Strained and Unstrained Step-index Glass Optical Fibers. *Appl Opt* (2010) 49:5076–80. doi:10.1364/AO.49.005076

Conflict of Interest: The authors declare that the research was conducted in the absence of any commercial or financial relationships that could be construed as a potential conflict of interest.

Publisher's Note: All claims expressed in this article are solely those of the authors and do not necessarily represent those of their affiliated organizations, or those of the publisher, the editors and the reviewers. Any product that may be evaluated in this article, or claim that may be made by its manufacturer, is not guaranteed or endorsed by the publisher.